Essential roles of $G\alpha_{12/13}$ signaling in distinct cell behaviors driving zebrafish convergence and extension gastrulation movements

Fang Lin,[1] Diane S. Sepich,[2] Songhai Chen,[1] Jacek Topczewski,[2,3] Chunyue Yin,[2] Lilianna Solnica-Krezel,[2] and Heidi Hamm[1]

[1]Department of Pharmacology, Vanderbilt University Medical Center, Nashville, TN 37232
[2]Department of Biological Sciences, Vanderbilt University, Nashville, TN 37235
[3]Department of Pediatrics, Northwestern University, Feinberg School of Medicine, Children's Memorial Institute for Education and Research, Chicago, IL 60614

$G\alpha_{12/13}$ have been implicated in numerous cellular processes, however, their roles in vertebrate gastrulation are largely unknown. Here, we show that during zebrafish gastrulation, suppression of both $G\alpha_{12}$ and $G\alpha_{13}$ signaling by overexpressing dominant negative proteins and application of antisense morpholino-modified oligonucleotide translation interference disrupted convergence and extension without changing embryonic patterning. Analyses of mesodermal cell behaviors revealed that $G\alpha_{12/13}$ are required for cell elongation and efficient dorsalward migration during convergence independent of noncanonical Wnt signaling. Furthermore, $G\alpha_{12/13}$ function cell-autonomously to mediate mediolateral cell elongation underlying intercalation during notochord extension, likely acting in parallel to noncanonical Wnt signaling. These findings provide the first evidence that $G\alpha_{12}$ and $G\alpha_{13}$ have overlapping and essential roles in distinct cell behaviors that drive vertebrate gastrulation.

Introduction

Gastrulation is a pivotal phase of vertebrate development during which the body plan is established via a complex series of the morphogenetic movements. Vertebrate gastrulation consists of three main morphogenetic processes: epiboly, internalization of presumptive mesendoderm, and convergence and extension (C&E). In zebrafish gastrulae, C&E movements narrow the germ layers mediolaterally and elongate them anteroposteriorly to define embryonic axes. Mesodermal mediolateral cell intercalation, as well as directed dorsal and anterior cell migration contribute to this morphogenetic processes (Warga and Kimmel, 1990; Trinkaus et al., 1992; Jessen et al., 2002; Glickman et al., 2003; Ulrich et al., 2003). How this diversity of gastrulation cell behaviors is generated remains poorly understood.

Noncanonical Wnt signaling, an equivalent of the planar cell polarity signaling in *Drosophila melanogaster* (Wnt-PCP), is a major regulator of the mediolateral cell polarization required for cell intercalation in frog and fish, and fast dorsal migration in fish gastrulae (Keller, 2002; Myers et al., 2002b; Wallingford et al., 2002). Mutants of several genes involved in this pathway, such as *trilobite* (*strabismus*; Jessen et al., 2002), *knypek* (*glypican4/6*; Topczewski et al., 2001), *silberblick* (*wnt11*; Heisenberg et al., 2000) display shortened axis and defective mesodermal cell polarization. Recent evidence indicates that Heterotrimeric G proteins may participate in the Wnt/Ca^{2+} branch of the noncanonical pathway, which involves intracellular Ca^{2+} release and activation of PKC (Sheldahl et al., 1999; Malbon et al., 2001). The Wnt signaling pathway is activated by the binding of Wnt ligands to the Frizzled receptors, which have seven transmembrane domains, a structural characteristic of G protein–coupled receptors (GPCRs). There is evidence that like GPCRs, Frizzled receptors may activate G proteins to mediate their signal transduction. In cultured cells, coupling of the Frizzled receptor to $G\alpha_o$, $G\alpha_q$, and $G\alpha_t$ has been reported (Liu et al., 1999; Liu et al., 2001; Ahumada et al., 2002). In addition, it has been shown that G proteins are involved in Wnt signaling pathways that mediate gastrulation. Expression of pertussis toxin (which ADP-rybosylates $G\alpha_i$ and $G\alpha_o$ and uncouples them from their cognate receptors) disrupts tissue separation during *Xenopus laevis* gastrulation, an effect also seen with Xfz7 depletion. Moreover, PKC can rescue the defect in tissue separation in both Xfz7-depleted and PTX-injected

Correspondence to Lilianna Solnica-Krezel: lilianna.solnica-krezel@Vanderbilt.edu; or Heidi Hamm: heidi.hamm@vanderbilt.edu

Abbreviations used in this paper: C&E, convergence and extension; dpf, days postfertizilation; GPCR, G protein–coupled receptor; HEK, human embryonic kidney; hpf, hours postfertizilation; LWR, length to width ratio; MO, morpholino-modified oligonucleotide; Rok, Rho kinase; WT, wild-type.

The online version of this article contains supplemental material.

The Journal of Cell Biology, Vol. 169, No. 5, June 6, 2005 777–787
http://www.jcb.org/cgi/doi/10.1083/jcb.200501104

embryos, suggesting that PTX-sensitive G proteins and PKC are involved in *Xenopus* gastrulation movements (Winklbauer et al., 2001). In addition, PKC_{α} and PKC_{δ} are activated by Frizzled receptors, possibly through G proteins and Dishevelled to regulate C&E movements in *Xenopus* (Kuhl et al., 2001; Kinoshita et al., 2003). Furthermore, $G\alpha_o$ is required for both the canonical Wnt and PCP signaling in *Drosophila* (Katanaev et al., 2005). Recently, it has been reported that $G\beta\gamma$ subunits may also play important roles in C&E movements. In *Xenopus* gastrulae, inhibition of $G\beta\gamma$ signaling by overexpression of $G\alpha_i$ and $G\alpha_t$ (which sequester free $G\beta\gamma$) rescued C&E defects that resulted from activation of Wnt11/Xfz7 (Penzo-Mendez et al., 2003). In addition, inhibition of $G\beta\gamma$ signaling in the *Xenopus* dorsal marginal zone resulted in gastrulation arrest. However, exactly which $G\alpha$-proteins are involved in Wnt-PCP–mediated gastrulation remains unknown.

G proteins consist of four classes: $G\alpha_s$, $G\alpha_i$, $G\alpha_q$, and $G\alpha_{12/13}$ (Simon et al., 1991). $G\alpha_{12/13}$ subunits are the most divergent G protein family and have been implicated in numerous cellular processes such as Rho-mediated cytoskeletal rearrangements, thereby affecting cell shape and migration (Buhl et al., 1995; Gohla et al., 1999; Sugimoto et al., 2003). Studies in *Drosophila* indicate that $G\alpha_{12/13}$ signaling plays a role in gastrulation, as inactivation of the *Drosophila* $G\alpha_{12}$ homologue, *concertina,* impairs cell shape changes underlying mesoderm internalization during gastrulation (Parks and Wieschaus, 1991). In mice, disruption of $G\alpha_{13}$ gene led to embryonic death at midgestation, due to the failure of endothelial cells to form an organized vascular system (Offermanns et al., 1997). In addition, $G\alpha_{12/13}$ have been shown to induce primitive endoderm formation in mouse F9 cells (Lee et al., 2004). However, the role of $G\alpha_{12/13}$ in vertebrate gastrulation has not been analyzed.

Here, we used zebrafish as a model to investigate the role of $G\alpha_{12/13}$ in early vertebrate embryogenesis. Using dominant negative receptor blocking peptides and antisense morpholino oligonucleotides (MOs), we demonstrate that $G\alpha_{12}$ and $G\alpha_{13}$ have overlapping and essential roles in C&E. Cell movement analyses show that $G\alpha_{12/13}$ signaling regulates slow dorsal migration of lateral mesoderm cells independent of noncanonical Wnt signaling. In the notochord, $G\alpha_{12/13}$ are required for mediolateral cell intercalation, acting cell-autonomously, and likely in parallel to noncanonical Wnt signaling. Our studies for the first time suggest a central role for $G\alpha_{12/13}$ signaling in generating the diversity of gastrulation cell behaviors in vertebrate embryos.

Results

Cloning and characterization of zebrafish *gna12* and *gna13* genes

One gene encoding $G\alpha_{12}$ (referred to as *gna12*) and two paralogues (*gna13a* and *gna13b*) encoding $G\alpha_{13}$ were found in zebrafish. $G\alpha_{13}$a and $G\alpha_{13}$b share 81% identical and 91% similar amino acid residues with each other, and have 90–93% sequence similarity to human $G\alpha_{13}$. The zebrafish $G\alpha_{12}$ protein shares 81% identical and 91% similar amino acid residues with human $G\alpha_{12}$ (Fig. S1, available at http://www.jcb.org/cgi/content/full/jcb.200501104/DC1).

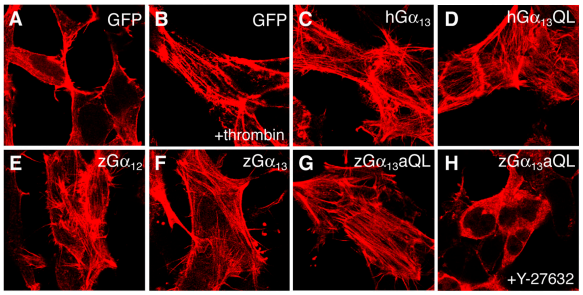

Figure 1. **Overexpression of human and zebrafish $G\alpha_{12/13}$ promoted stress fiber formation.** Stress fiber formation was determined in HEK 293 cells transiently transfected with cDNAs encoding GFP (A and B), WT human (C) or zebrafish (E and F), constitutively active human (D) or zebrafish (G and H) G-proteins. Cells were stimulated with (B) or without (A, and C–H) 10 nM thrombin for 10 min, and then stained with 0.17 μM Rhodamine-phalloidin. 10 μM Y-27632 was used to block Rho kinase activity (H).

In cultured cells, mammalian $G\alpha_{12/13}$ induce stress fiber formation via a RhoA/Rho kinase (Rok)-dependent pathway (Buhl et al., 1995; Gohla et al., 1998). To evaluate if zebrafish $G\alpha_{12/13}$ have similar activities, wild-type (WT) and constitutively active $G\alpha_{12/13}$ mutant proteins were transiently expressed in human embryonic kidney (HEK) cells. Cells overexpressing either WT human or zebrafish $G\alpha_{12}$ or $G\alpha_{13}$ (Fig. 1, C, E, and F) or constitutively active human or zebrafish $G\alpha_{13}$ (Fig. 1, D and G) displayed stress fibers even in the absence of agonist stimulation. Formation of stress fibers was blocked by pretreatment with 10 μM of Rok inhibitor, Y-27623 (Fig. 1 H; Uehata et al., 1997). These results indicate that like their human counterparts, zebrafish $G\alpha_{12/13}$ can promote actin rearrangements in cultured cells, through a RhoA/Rok-dependent pathway.

Expression of zebrafish *gna12* and *gna13* genes

Whole-mount in situ hybridization revealed that *gna12* and both *gna13* transcripts are maternally deposited (Fig. 2, A–C). Accordingly, high levels of $G\alpha_{12}$ and $G\alpha_{13}$ proteins were detected at the 8 cell stage by immunohistochemistry using antibodies that recognize the last 11 aa of $G\alpha_{12}$ or $G\alpha_{13}$ (not depicted). During blastula and gastrula stages, transcripts of all

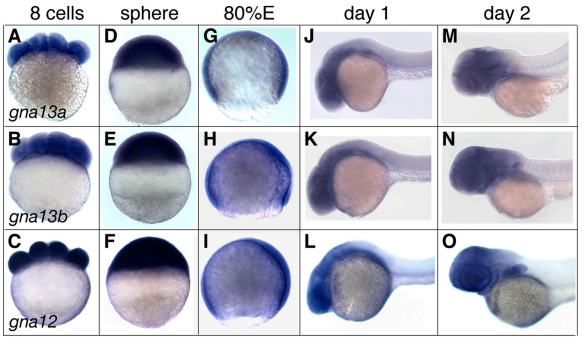

Figure 2. **Expression of Zebrafish *gna12* and *gna13* genes.** Expression of *gna12*, *gna13a*, and *gna13b* genes during zebrafish embryogenesis was detected by whole mount in situ hybridization. All embryos are shown in lateral view; animal pole is up for 8 cell (A–C), sphere stage (D–F), and 80% epiboly (G–I) embryos; dorsal is toward the right for 80% epiboly; anterior to the left for embryos at 1 and 2 dpf (J–O).

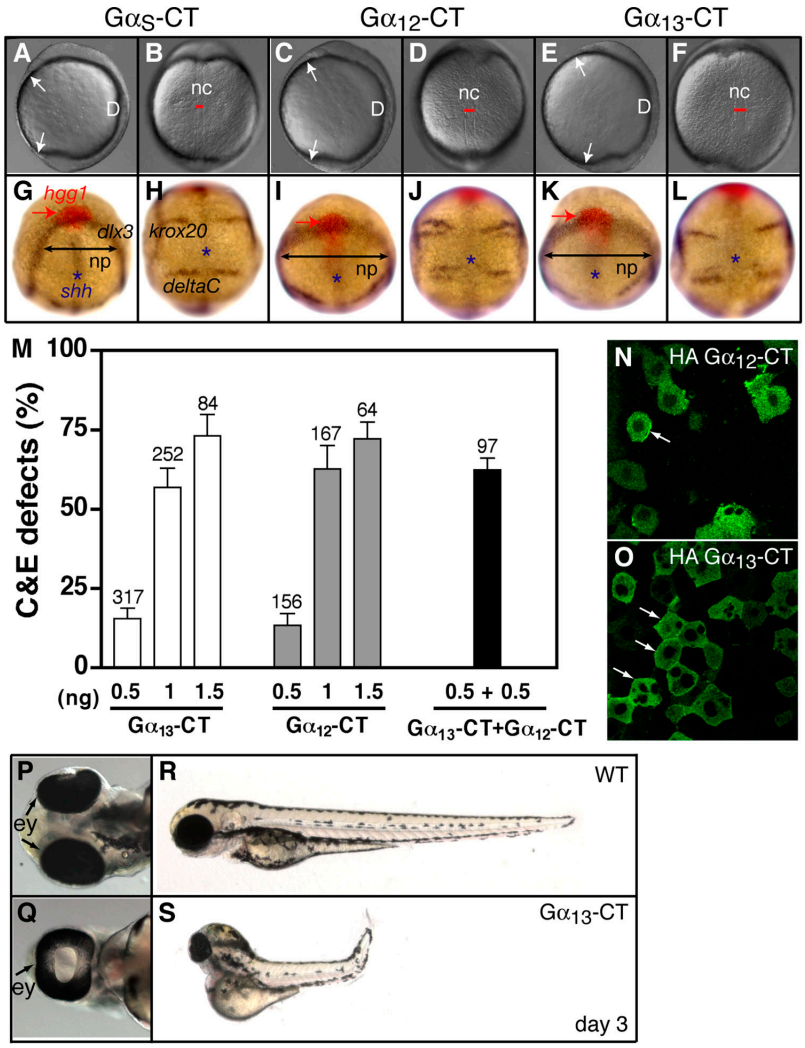

Figure 3. **Dominant negative Gα$_{12/13}$ CT-peptides disrupt C&E during zebrafish gastrulation.** (A–L) Embryos expressing the COOH-terminal peptides of Gα$_s$, Gα$_{12}$, or Gα$_{13}$ at 1–2 somite stage. (A–F) Images of live embryos. D, dorsal; nc, notochord; white arrows point to the anterior and posterior limits of the anteroposterior embryonic axis; lateral view (A, C, and E); dorsal views, animal pole up (B, D, and F). (G–L) Expression of prechordal plate (*hgg1*, red), neural plate boundary (*dlx3*), rhombomeres 3 and 5 (*krox20*), midline (*shh*), somites (*deltaC*) markers. Dorsoanterior view (G, I, and K); dorsal view (H, J, and L); (*), marks notochord; np, neural plate. (M) Frequencies of embryos overexpressing CT-peptides with C&E defects. Number on the top of the bar indicates the number of injected embryos from several separate experiments. (N and O) Confocal images of embryos overexpressing HA-tagged Gα$_{12}$-CT or Gα$_{13}$-CT immunostained with anti-HA antibody. White arrows indicate enrichment of staining on the membrane. (P–S) WT (P and R) and Gα$_{13}$-CT expressing (Q and S) embryos at 3 dpf. ey, eye; ventral (P and Q), and lateral views (R and S), anterior to the left.

three genes are present ubiquitously throughout embryo (Fig. 2, D–I). By 1–2 d postfertilization (dpf), the expression becomes confined to anterior body regions (Fig. 2, J–O).

Interference with Gα$_{12/13}$ function disrupts gastrulation movements

To investigate the function of the zebrafish Gα$_{12}$ and Gα$_{13}$ proteins in embryonic development, we used two strategies to inhibit Gα$_{12/13}$ signaling. First, we overexpressed peptides encoding the last 11 or 50 COOH-terminal aa of both proteins, referred to as CT-peptides. The COOH-terminal region of G protein α subunits has been shown to be a major binding site of G proteins to their cognate receptors (Hamm, 1998). Overexpression of CT-peptides in cells or mice has been shown to block competitively the receptor sites that normally bind to G proteins, leading to specific blockade of the respective Gα signaling (Akhter et al., 1998; Gilchrist et al., 1999, 2001; Feldman et al., 2002; Arai et al., 2003). Strikingly, compared with their control siblings, embryos injected with synthetic RNAs encoding the CT-peptides (the last 11 aa) of Gα$_{12}$ or Gα$_{13}$ (Gα$_{12}$-CT, Gα$_{13}$-CT) exhibited shortened body axes with broader notochords and somites (Fig. 3, C–F), as well as delayed epiboly (unpublished data). At 3 dpf, these embryos remained shorter, and frequently displayed synophthalmia or cyclopia (Fig. 3, P–S), phenocopying defects often associated with defective C&E movements in *silberblick* (*wnt11*) or *trilobite* (*strabismus*) noncanonical Wnt signaling mutants (Heisenberg et al., 2000; Jessen et al., 2002). Examination of expression patterns of tissue specific markers confirmed that embryos expressing Gα$_{12}$-CT or Gα$_{13}$-CT displayed broader neural plate and notochord. Furthermore, prechordal mesendoderm was positioned more posteriorly with respect to the anterior edge of the neural plate during early segmentation stage (Fig. 3, I–L), suggestive of impaired anterior migration of this cell population (Heisenberg et al., 2000; Topczewski et al., 2001; Jessen et al., 2002; Marlow et al., 2002). Both severity and penetrance of the observed phenotypes increased with the dose of Gα$_{12}$-CT or Gα$_{13}$-CT RNAs. Whereas 15% of embryos injected with 0.5 ng Gα$_{12}$-CT or Gα$_{13}$-CT RNA showed morphology consistent with impaired C&E movements, 60% and 70% of embryos injected with 1 and 1.5 ng Gα$_{12}$-CT or Gα$_{13}$-CT RNA showed similar C&E defects, respectively (Fig. 3 M). These data suggest that Gα$_{13}$ and Gα$_{12}$ both function in C&E movements. In contrast, C&E defects were not observed in embryos injected

with up to 2 ng RNA encoding $G\alpha_s$ CT peptide (a different class of Gα subunit; Fig. 3, A, B, G, and H), suggesting the specific involvement of $G\alpha_{12/13}$ in gastrulation. Similarly, overexpression of the COOH-terminal 50 aa of $G\alpha_{12}$ or $G\alpha_{13}$, conjugated with HA-tag, produced similar gastrulation defects (not depicted). Anti-HA immunohistochemistry showed these longer peptides were robustly expressed in the cytosol, with slight enrichment on the membrane (Fig. 3, N and O).

In a complementary approach, we used antisense MOs (Nasevicius and Ekker, 2000) to block $G\alpha_{12/13}$ translation in zebrafish. The endogenous $G\alpha_{12}$ and $G\alpha_{13}$ in zebrafish blastulae were detected predominantly on the cell membranes and in a punctate pattern in the cytosol (Fig. 4, A and C). When embryos were injected with MO (4 ng) targeting *gna12* transcript, the expression of $G\alpha_{12}$ was strongly reduced (Fig. 4 B). Likewise coinjection of MOs targeting *gna13a* and *gna13b* transcripts (4 ng each) decreased the level of both $G\alpha_{13}$ proteins at late blastula stage (Fig. 4 D). Together, these results demonstrated that the MOs we designed effectively blocked *gna12* or *gna13* translation. Injections of up to 20 ng/embryo of MO against any single *gna12/13* transcript (either *gna13a* or *gna13b* alone or in combination, or *gna12* alone) had no obvious effect on embryonic development probably due to functional redundancy between $G\alpha_{12}$ and $G\alpha_{13}$ in zebrafish (Fig. 4 E and not depicted). However, when the embryos were injected with a mixture of MOs against *gna13a*, *gna13b*, and *gna12* (3MOs, 4 ng each), 76% of embryos showed impaired C&E movements as judged by alteration of embryonic morphology and gene expression patterns (Fig. 4, F and H; $n = 214$). The phenotypes resulting from MO interference were very similar to those caused by overexpression of CT-peptides. To test whether the above gastrulation defects are due to specific interference of MOs with $G\alpha_{12/13}$ function, we coinjected a subthreshold dose of human *GNA13* RNA along with three MOs. Because the MO targeted nucleotide sequence of the human gene diverges from the sequences of zebrafish homologues, it cannot be blocked by the MOs used here. Injection of 10–20 pg human *GNA13* RNA had no obvious effect on zebrafish morphogenetic movements of epiboly and C&E (unpublished data). However, when this amount of human *GNA13* RNA was coinjected with the combination of the three MOs, the percentage of embryos with gastrulation defects decreased from 76% to 20% (Fig. 4 H). Whereas 75% of embryos ($n = 120$) injected with the three MOs exhibited a very short body axis, and some degree of brain degeneration by 1 dpf, coexpression of human $G\alpha_{13}$ largely suppressed the axis extension defects with 75% embryos showing an almost normal body length (Fig. 4, I–K; $n = 138$). As shown by morphometric analysis, embryos coinjected with three MOs exhibited a reduced body length of 2015 ± 50 μm ($n = 22$), compared with embryos injected with a single MO (2962 ± 10 μm, $n = 10$). By contrast, embryos coinjected with human *GNA13* RNA and three MOs showed significantly restored body length (2432 ± 47 μm, $n = 22$, $P = 7.6 \times 10^{-9}$). However, only modest suppression of brain degeneration was observed. These results indicate that the morphogenetic defects are a specific consequence of the interference with $G\alpha_{12/13}$ function, whereas the neural degeneration phenotype might be a nonspecific defect, often associated with MO injection (Nasevicius and Ekker, 2000). In addition, zebrafish and human $G\alpha_{13}$ share a conserved activity in gastrulation. Interestingly, the effects of CT peptides and MOs were synergistic. Although very few embryos showed C&E defects when injected with moderate doses of either $G\alpha_{13}$-CT RNA (9%, 500 pg, $n = 126$) or *gna13a*-MO (0%, 5 ng, $n = 120$), coinjection of both resulted in 65% embryos displaying C&E defects (65%, $n = 73$). Comparable results were found when embryos were coinjected with $G\alpha_{13}$-CT RNA and *gna13b*-MO or $G\alpha_{12}$-CT RNA and *gna12*-MO (unpublished data).

Similar C&E defects were also observed in embryos overexpressing WT $G\alpha_{13}$a, $G\alpha_{13}$b, or $G\alpha_{12}$ proteins, and occurred in a dose-dependent manner (Fig. 4 G and not depicted). Co-injection of $G\alpha_{12/13}$ specific MOs suppressed gastrulation defects resulting from overexpression of $G\alpha_{12/13}$ (not depicted). This indicates that the phenotypes caused by $G\alpha_{12/13}$ are due to specific interference with their functions, and provides further support for the effectiveness of these MOs. Together these results show that both reduction and excess $G\alpha_{12/13}$ function impair the C&E gastrulation process.

Interference with $G\alpha_{12/13}$ function does not alter cell fate specification during gastrulation

Gastrulation defects might be a consequence of altered embryonic patterning and consequent changes in cell movements, or might be due to defects in cell movements alone (Myers et al., 2002b). Therefore, we tested whether dorsoventral patterning is affected in $G\alpha_{12/13}$-CT or MO injected embryos by analyzing expression of dorsoventral patterning genes, *bmp4* and *chordin* (Hammerschmidt and Mullins, 2002). Our results revealed that *bmp4* expression was not altered in early and late gastrulae injected with three MOs (Fig. 4 M, $n = 34$, and not depicted). Likewise, expression of *chordin* gene encoding a Bmp antagonist was confined to its normal dorsal expression domain during early gastrulation in embryos injected with the combination of 3MO (Fig. 4 O, $n = 32$), or with RNAs encoding $G\alpha_{12/13}$-CT peptides (not depicted). Moreover, embryos injected with CT peptide RNA or 3MO displayed normal expression of several cell type specific markers at late gastrulation, consistent with normal cell fate specification (Fig. 3, I–L; Fig. 4 F). Finally, cell tracing experiments revealed that the labeled lateral mesodermal cells acquired somitic fates in $G\alpha_{12/13}$-depleted embryos (not depicted), consistent with their positions in the early gastrula (Sepich et al., 2000). Based on these results, we conclude that morphogenetic defects observed in $G\alpha_{12/13}$ depleted embryos are likely not associated with significant patterning or cell fate changes during gastrulation.

$G\alpha_{12/13}$ are required for efficient directed cell migration during early dorsal convergence movements

Shortened anteroposterior and enlarged mediolateral dimensions of the embryonic axes in $G\alpha_{12/13}$-depleted gastrulae could be a consequence of defective C&E movements (Sepich et al., 2000). Recent studies reveal that convergence movements in

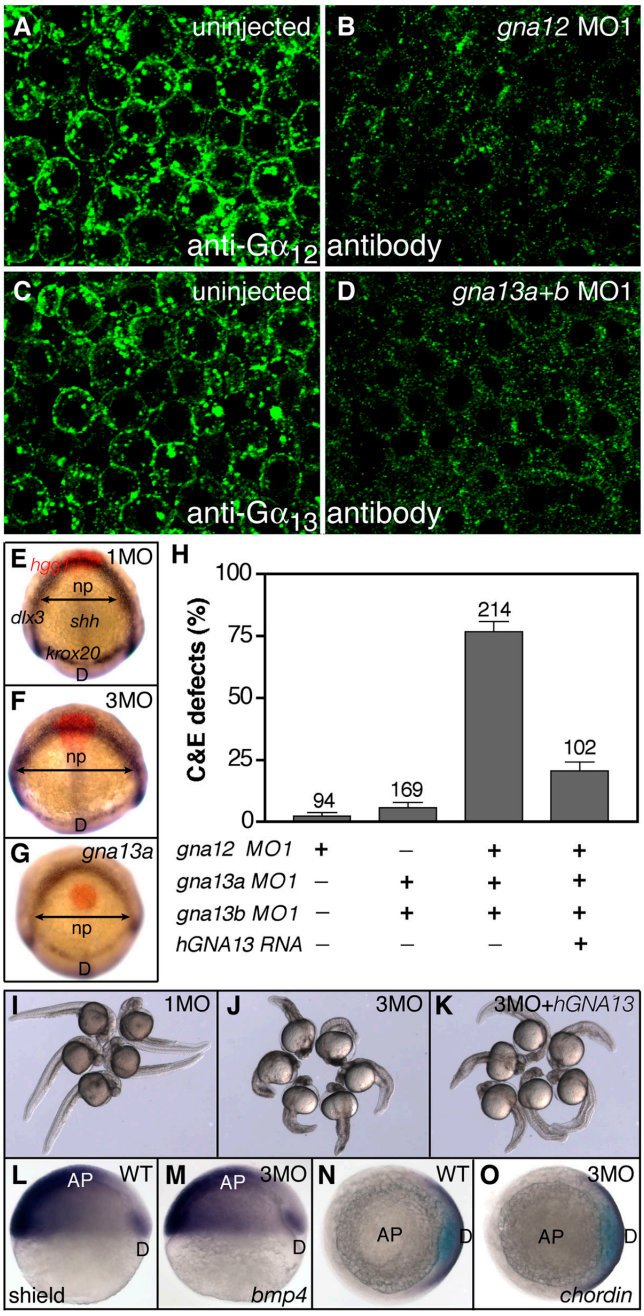

Figure 4. **$G\alpha_{12/13}$-depleted embryos exhibit C&E defects without changes in dorsoventral patterning.** (A–D) Confocal immunostaining images of blastoderm injected with MOs against *gna12* (B) or *gna13a* and *gna13b* (D; 16 embryos, from two independent experiments). (E–G) In situ hybridization with *hgg1* (red), *dlx3*, *shh*, and *krox20* of embryos injected with either a single MO (E; 1MO) or a combination of three MOs against $G\alpha_{12/13}$ (F; 3MO), or embryos overexpressing $G\alpha_{13}$a (G; 100 pg) at 1 somite stage. Animal pole view, dorsal toward the bottom. np, neural plate; D, dorsal. (H) Frequencies of embryos with C&E defects after the injection of MOs alone or with human *GNA13* RNA. Number on top of the bar indicates the number of injected embryos. Data were compiled from several separate experiments. (I–K) Group images of live embryos injected with single (I; 1MO) or three (J; 3MO) MOs, or 3MO together with human *GNA13* RNA (K) at 25 h postfertilization (hpf). (L–O) Expression of *bmp4* (L and M; lateral view, dorsal on the right), and *chordin* (N and O, animal view) in WT and 3MO-injected embryos at early gastrulation (6 hpf). D, dorsal; AP, animal pole.

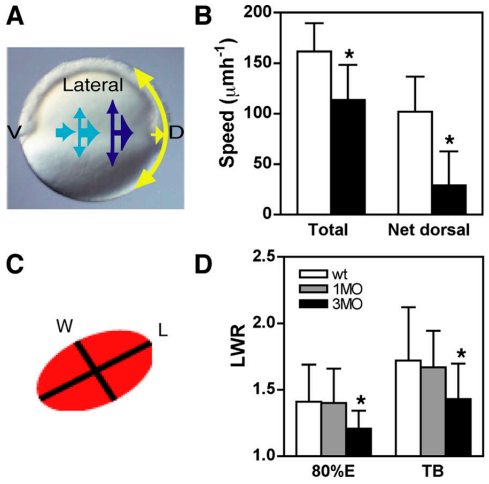

Figure 5. **$G\alpha_{12/13}$ signaling is required for efficient directed dorsal migration.** (A) Domains of C&E movements in zebrafish gastrulae (Myers et al., 2002b). Yellow arrows in the dorsal region indicate strong extension movements with little convergence. Light and dark blue arrows indicate domains of slow and fast C&E, respectively. (B) Total and net dorsal speed of lateral mesodermal cells at 80% epiboly were determined in WT and 3MO-injected embryos. Net speed in these experiments is somewhat higher than previously reported for this domain (Jessen et al., 2002). (C) A schematic representation of the method used to measure cell shape (LWR, length-to-width ratio). (D) LWR of lateral mesodermal cells in WT, 1MO-, or 3MO-injected embryos at 80% epiboly (8.5 hpf) and tailbud (TB, 10 hpf) stages.

zebrafish mesoderm are accomplished by a stereotyped sequence of cell behaviors, including slow and fast directed cell migration (Jessen et al., 2002). To investigate if any of the convergence cell behaviors were altered in $G\alpha_{12/13}$-depleted embryos, we performed Nomarski time-lapse analyses in WT (6 embryos, 144 cells) and 3MO-injected (6 embryos, 134 cells) embryos at midgastrulation. Analysis of total cell speed, accounting for movement in all directions, revealed that in $G\alpha_{12/13}$-depleted gastrulae, cells moved at a reduced speed (70% of WT total speed; $P = 9.8 \times 10^{-27}$; Fig. 5 B). Interestingly, the net dorsal speed of $G\alpha_{12/13}$-depleted cells was especially strongly compromised, accounting only for 28% of the WT net dorsal speed ($P = 2.1 \times 10^{-13}$, Fig. 5 B). Further analysis of cell migration paths revealed that, similar to the WT cells, $G\alpha_{12/13}$-depleted cells migrated predominantly dorsally (Fig. 6 A). However, compared with WT, these cells more frequently changed their movement direction (Fig. 6, A and B), at the expense of movement in the dorsal direction (Fig. 6 C). To determine how efficiently WT and 3MO cells corrected their path direction when they were off-course, we examined cells moving toward dorsal, animal, ventral or vegetal direction (± 15°) and assayed the direction of their next step (Fig. 6, D–G). We found that in WT embryos, cells moving dorsally largely maintained this direction in the next step. Moreover, WT cells that had been moving in the animal or vegetal direction turned toward dorsal in the next movement step, very few cells from these populations moved away from dorsal. By contrast, equivalent cell populations in embryos injected with 3MO were less persistent in dorsal movement (Fig. 6 D). Moreover, when these cells moved in animal or vegetal direction, they less frequently corrected their movement toward dorsal compared

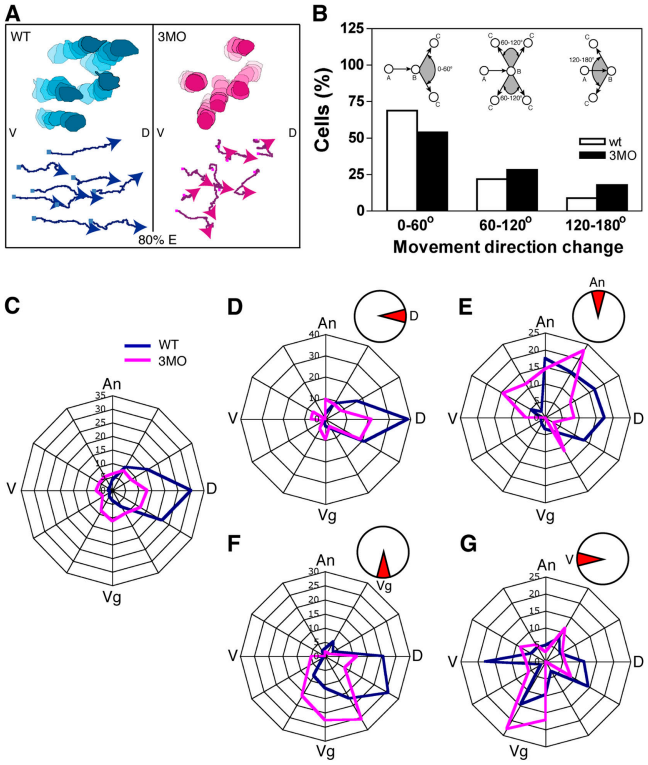

Figure 6. **$G\alpha_{12/13}$ signaling is essential for error-free directed migration.** Nomarski time-lapse analyses were performed on lateral mesodermal cells of WT and 3MO-injected embryos at 80% epiboly. (A) Representative cell shape changes and migration paths of a few cells from a single embryo. Cell shape was drawn for these selected cells at every 2.5-min interval. (B) Movement direction change in degrees. (Inset) A–C represent positions of the cell analyzed. A cell establishes a direction from position A to B, then moves to position C. Movement direction change presents angle change of position B to C. (C–G) Actual directions of cell movement (every 60-s interval, grouped into 30° sectors) shown in percentage of cells in WT (blue line) and 3MO-injected embryos (violet line). Directions of all cell movement events throughout the time lapse (C; 3,937 events in WT, 626 events in 3MO-injected embryo). Cell movement directions during the next 60-s interval of the population of cells moving toward dorsal (D; WT, 1,139 events; 3MO, 74 events), animal (F; WT, 149 events; 3MO, 35 events), vegetal (E; WT, 151 events; 3MO, 62 events) or ventral (G; WT, 62 events; 3MO, 35 events) direction (± 15°). Insets: starting directions. An, animal; Vg, vegetal; D, dorsal; V, ventral.

with WT cells (Fig. 6, E and F). Cells moving ventrally made large turns, and no clear difference is apparent between WT and 3MO cells (Fig. 6 G). Consequently, cells in $G\alpha_{12/13}$-depleted gastrulae migrated less efficiently toward dorsal. In support of the notion that this defect is specific to the depletion of $G\alpha_{12/13}$ proteins, cells in embryos injected with an equivalent dose of *gna13a*-MO (12 ng) migrated dorsally at comparable speed to WT cells (unpublished data). Together, these studies revealed that $G\alpha_{12/13}$ function is required for directed dorsal migration underlying the early, slow convergence movements of lateral mesodermal cells.

Next, we aimed to identify the cellular basis of this movement defect. We analyzed the shapes (length to width ratio [LWR], where the length and width represent the largest measurable distances along each cellular axis, Fig. 5 C) of $G\alpha_{12/13}$-depleted lateral mesodermal cells at mid- and late-gastrulation. In WT embryos at midgastrulation, lateral mesodermal cells exhibited an average LWR of 1.41 ± 0.28 (250 cells, 6 embryos), and became elongated at late gastrulation with LWR of 1.72 ± 0.4 (487 cells, 16 embryos, $P = 3.2 \times 10^{-32}$; Fig. 5 D), in agreement with previous findings (Topczewski et al., 2001; Jessen et al., 2002). Cells in embryos injected with a high dose of a single MO (12 ng, any of the three) exhibited shapes not significantly different from those observed in WT embryos at equivalent stages, at midgastrulation (with LWR of 1.4 ± 0.26, 182 cells, 6 embryos; P = 0.7) and at tailbud (with LWR of 1.67 ± 0.28, 102 cells, 6 embryos, P = 0.2; Fig. 5 D). In contrast, in embryos injected with the combination of three MOs against *gna12/13* transcripts, mesodermal cells were significantly less elongated at midgastrulation with LWR of 1.2 ± 0.14 (443 cells, 9 embryos, $P = 7.0 \times 10^{-24}$). At late gastrulation, these cells remained rounder than equivalent cells in the control embryos with LWR of 1.43 ± 0.27 (158 cells, 6 embryos, $P = 4.3 \times 10^{-24}$; Fig. 5 D). These results revealed that $G\alpha_{12/13}$ signaling mediates cell elongation associated with the early convergence movements. Notably, the requirement for $G\alpha_{12/13}$ function for moderate elongation of lateral mesodermal cells is manifest already at midgastrulation, and thus before the noncanonical Wnt signaling is thought to become essential during convergence (Jessen et al., 2002). Collectively, these results indicate that $G\alpha_{12/13}$ function is required for normal cell elongation and effective directed migration during C&E movements.

Interference with $G\alpha_{12/13}$ function disrupts mediolateral cell intercalation

Mediolaterally oriented intercalation of cells at the dorsal midline drives robust axial extension in zebrafish (Crawford et al., 2003; Glickman et al., 2003) and *Xenopus* gastrulae (Shih and Keller, 1992). During gastrulation, notochord precursor cells elongate, align mediolaterally and intercalate between one another to lengthen the notochord anteroposteriorly and narrow its mediolateral dimension, decreasing from the initial width of 4–5 to 1–2 cells (Glickman et al., 2003). To investigate whether $G\alpha_{12/13}$ signaling is required for mediolateral intercalation of midline cells, we analyzed shape (LWR) and orientation of notochord cells at the 4 and 6 somite stage. We found that at the 4 somite stage, the WT notochord was one to two cells wide, and cells were aligned mediolaterally (at an average angle of 6 ± 5° relative to a line perpendicular to the embryonic axis as represented by the notochord) and were well elongated with LWR of 3.24 ± 1.19 (166 cells, 6 embryos; Fig. 7, A–C). At the 6 somite stage, notochord cells were further elongated with LWR of 4.84 ± 1.92 and aligned mediolaterally with an angle of 4 ± 3° (241 cells, 8 embryos; Fig. 7, A and B). In contrast, in $G\alpha_{12/13}$-depleted embryos at the 4 somite stage, the notochord was two or three cells wide revealing an intercalation defect, and these cells were rounder, exhibiting an average LWR of 2.25 ± 0.79 (254 cells, 9 embryos, $P = 3.3 \times 10^{-18}$; Fig. 7, A and D), however, these cells still aligned mediolaterally but at a slightly greater angle of 11 ± 12° ($P = 4.2 \times 10^{-9}$; Fig. 7, B and D). At the 6 somite stage, notochord cells in $G\alpha_{12/13}$-depleted embryos continued to show impaired elongation and orientation defects with LWR of 2.95 ± 1.2 and angle of 8 ± 8° relative to the me-

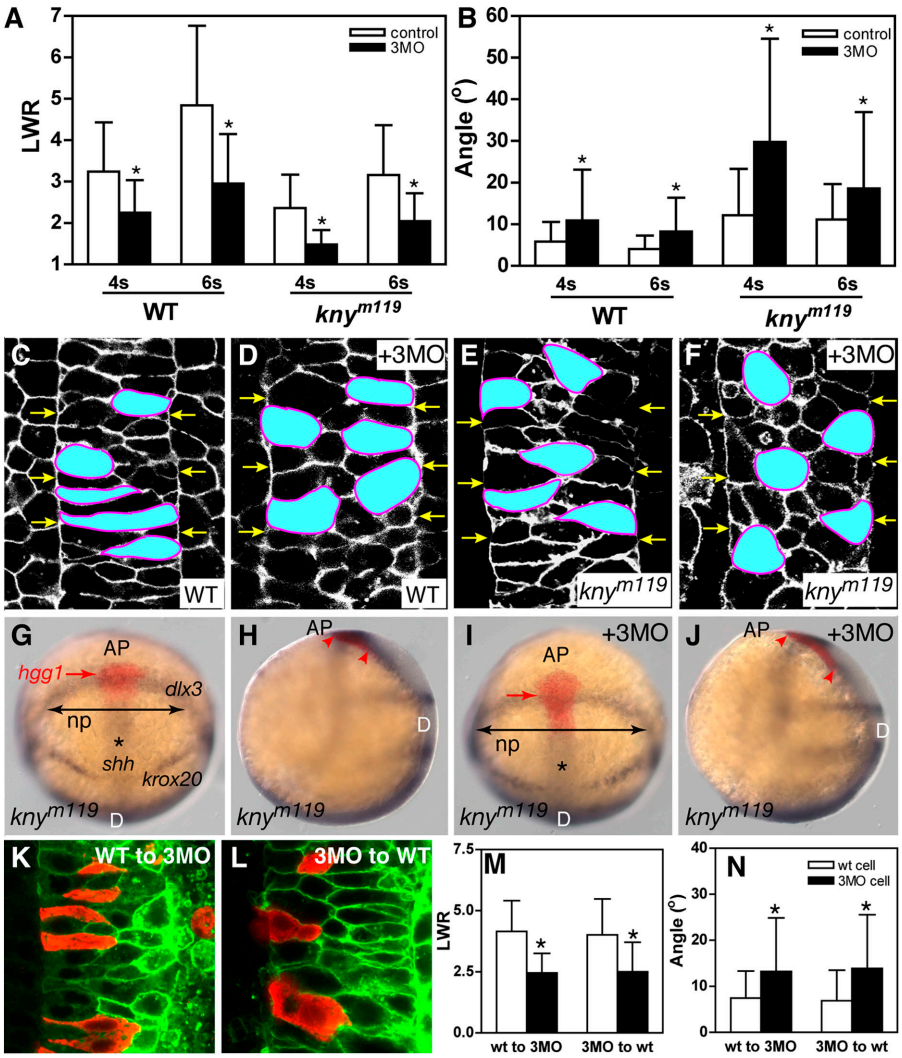

Figure 7. **$G\alpha_{12/13}$ signaling is autonomously required for efficient mediolateral intercalation and interacts with Wnt signaling.** (A and B) LWR of notochord cells (A) and the angle of the long axis of notochord cells relative to a line perpendicular to the embryonic axis (B) in WT or *kny*^{m119} embryos injected with *mgfp* RNA alone (control) or with 3MOs at 4 and 6 somite stages. (C–F) Representative images of notochord of WT or *kny*^{m119} embryos at 4 somite stage injected with *mgfp* RNA alone or with 3MOs. Yellow arrows indicate notochord boundary and a few notochord cells in each group were artificially filled with light blue for illustration, their membrane were outlined with violet lines. (G–J) 1-somite *kny*^{m119} embryos (G and H) and *kny*^{m119} embryos injected with 3MOs (I and J) were labeled with *hgg1*, *dlx3*, *krox20*, and *shh*. Dorsoanterior view (G and I); lateral view (H and J); (*), marks notochord. Black lines indicate the width of the neural plate; red arrows show prechordal plate and red arrowheads point the most anterior and posterior extent of the prechordal plate, which is abnormally elongated in 3MO-injected embryos. (K and L) Representative confocal images of transplanted WT (K) and 3MO-injected (L) donor-derived notochord cells (red), surrounded by mGFP labeled host cells (green). (M and N) LWR and the angle of transplanted and donor notochord cells with respect to a line perpendicular to the embryonic axis.

diolateral axis (202 cells, 6 embryos, $P = 5.1\times 10^{-31}$; Fig. 7, A and B). These results indicate $G\alpha_{12/13}$ signaling is also required for elongation and intercalation of axial mesodermal cells, and consequently for C&E of embryonic axis.

To test the cell-autonomy of $G\alpha_{12/13}$ function in notochord C&E, we transplanted cells at blastula stage from donors injected with rhodamine-dextran alone or with 3MOs into WT hosts injected with *mgfp* RNA and 3MOs or *mgfp* RNA alone, and determined shape and orientation of cell bodies in notochord at 4 somite stage. We found that transplanted $G\alpha_{12/13}$-depleted cells exhibited rounder shapes (with LWR of 2.50 ± 1.21, 39 cells, 7 embryos, $P = 4.49 \times 10^{-9}$) and more random orientation (with angle of 13.91 ± 11.66°, $P = 7.0 \times 10^{-4}$) even in WT environment (with LWR of 4.01 ± 1.47 and angle of 6.84 ± 6.66°, 167 cells; Fig. 7, K, M, and N). Conversely, WT cells displayed normal elongated shape and orientation (with LWR of 4.15 ± 1.26 and angle of 7.43 ± 5.89°, 43 cells, 5 embryos; Fig. 7, K, M, and N) even in $G\alpha_{12/13}$ signaling-depleted hosts (with LWR of 2.45 ± 0.8 and angle of 13.21 ± 11.65°, 157 cells, $P = 3.3 \times 10^{-11}$ for LWR and $P = 1.6 \times 10^{-5}$ for angle compared with WT cells; Fig. 7, L–N). These results reveal a cell-autonomous requirement for $G\alpha_{12/13}$ in mediolateral cell elongation during C&E of notochord.

The relationship between $G\alpha_{12/13}$ and the noncanonical Wnt signaling during zebrafish gastrulation

The noncanonical Wnt signaling pathway mediates mediolateral cell polarization underlying normal C&E movements (Keller, 2002; Myers et al., 2002b; Wallingford et al., 2002). The morphological changes in embryos with altered $G\alpha_{12/13}$ signaling are strikingly similar to those reported for mutants of *slb (wnt11)* and *knypek (glypican4/6)* that resulted from the disruption of the noncanonical Wnt signaling (Heisenberg et al., 2000; Topczewski et al., 2001). Moreover, $G\alpha_{12/13}$-depleted mesodermal cells also exhibited impaired cell elongation during late gastrulation (Fig. 5), similar to embryos overexpressing dominant negative Rok2 and *trilobite* and *knypek* mutants (Topczewski et al., 2001; Jessen et al., 2002; Marlow et al., 2002). However, our studies showed that $G\alpha_{12/13}$ are required for two types of directed cell migration for which noncanonical signaling does not appear to be required: early slow convergence and epiboly (Fig. 5; unpublished data), suggesting that

$G\alpha_{12/13}$ mediate these movements independent of Wnt signaling. To elucidate the functional relationship between $G\alpha_{12/13}$ signaling and noncanonical Wnt signaling during gastrulation, we analyzed the effect of modulation of $G\alpha_{12/13}$ signaling on noncanonical Wnt signaling mutant phenotypes.

The small GTPase Rho, is the main effector of $G\alpha_{12}$ and $G\alpha_{13}$ (Buhl et al., 1995) and is also implicated in noncanonical Wnt signaling (Habas et al., 2001). Accordingly, Rho downstream mediator Rok2 can partially suppress the *slb (wnt11)* gastrulation defects (Marlow et al., 2002). To address whether zebrafish $G\alpha_{12/13}$ can modulate Wnt11 signaling during gastrulation, we injected RNAs encoding $G\alpha_{13}$ to enhance, or $G\alpha_{13}$-CT to inhibit the function of $G\alpha_{13}$, in homozygous *slb (wnt11)*$^{tz216/tz216}$ embryos (Heisenberg et al., 2000). However, neither various levels of excess nor deficit of $G\alpha_{13}$ signaling could suppress the gastrulation defects in *slb (wnt11)*$^{-/-}$ embryos. Rather, both perturbations of $G\alpha_{13}$ signaling exacerbated the *slb (wnt11)*$^{-/-}$ phenotype (unpublished data). We also performed molecular epitasis experiments by injecting embryos obtained from *kny*^{m119} heterozygotes, carrying a null mutation in the *glypican 4/6* gene (Topczewski et al., 2001), with a small dose of synthetic RNAs encoding $G\alpha_{13}$ or MOs against *gna13* or three MOs against both *gna13* and *gna12*. Neither overexpression of $G\alpha_{13}$ nor down-regulation of $G\alpha_{13}$ signaling suppressed *kny*$^{(-/-)}$ C&E defects. Instead, depletion of $G\alpha_{12/13}$ signaling by injection with three MOs enhanced the *kny*$^{(-/-)}$ defects of neuroectoderm convergence and of anterior prechordal mesendoderm migration (Fig. 7, G–J). Finally, the expression pattern of *wnt11*, *kny*, or *tri* was unchanged in embryos with excess or deficit of $G\alpha_{12/13}$ signaling (unpublished data). These results are consistent with the notion that $G\alpha_{12/13}$ and noncanonical Wnt signaling functionally interact during zebrafish gastrulation, likely acting in parallel pathways.

To address the cellular basis of the exacerbated C&E defects in *kny* mutants with compromised $G\alpha_{12/13}$ signaling, we focused on cell intercalation that drives notochord convergence and extension (see above; Glickman et al., 2003). Our previous studies showed that axial mesoderm C&E is impaired in *kny* mutants (Topczewski et al., 2001), although the underlying cell defects have not been investigated. Compared with WT embryos, notochord cells in *kny* mutants showed impaired elongation and orientation at the 4 somite stage with LWR of 2.37 $\pm$ 0.8 and angle of 12 $\pm$ 11° (269 cells, 8 embryos) and at 6 somite stage with LWR of 3.16 $\pm$ 1.2 and angle of 11 $\pm$ 9° (256 cells, 7 embryos; Fig. 7, A, B, and E). These results suggest that *kny* not only mediates lateral cell elongation, it also contributes to midline cell alignment. To test whether $G\alpha_{12/13}$ signaling functions in addition to *kny* in midline cells, embryos obtained from *kny* heterozygous parents were injected with 3MOs and notochord cells from *kny* homozygous mutant embryos were analyzed. Notably, deficit of $G\alpha_{13}$ signaling in *kny* homozygous mutant embryos exacerbated defects in notochord cells relative to *kny* mutant embryos. At 4 somite stage, the notochord cells were much rounder with LWR of 1.48 $\pm$ 0.35 (220 cells, 7 embryos, $P = 1.7\times 10^{-44}$ compared with *kny* embryos) and lacked proper mediolateral alignment with an angle of 30 $\pm$ 25° ($P = 9.3\times 10^{-20}$; Fig. 7, A, B, and F). Similar results were found in embryos at 6 somite stage (Fig. 7, A and B). Moreover, we also performed molecular epistasis experiments by injecting embryos obtained from *kny* heterozygotes with a small dose of *gna13a* RNA or MOs against *gna13* or 3MOs against both *gna13* and *gna12*. Overexpression of $G\alpha_{13}$ did not suppress *kny* C&E defects (not depicted), whereas depletion of $G\alpha_{12/13}$ signaling by injection with 3MO enhanced these defects (Fig. 7, G–J).

Collectively, these results suggest that $G\alpha_{12/13}$ do not simply act as the downstream effectors of *slb* or *kny* to mediate C&E movements. However, $G\alpha_{12/13}$ appears to functionally interact with noncanonical Wnt signaling to influence cell movements, likely acting through a parallel pathway.

Discussion

In this study, we have provided evidence that $G\alpha_{12}$ and $G\alpha_{13}$ play overlapping and essential roles during zebrafish gastrulation. Thus, overexpression of $G\alpha_{12/13}$ CT-peptides to uncouple $G\alpha_{12/13}$ from their cognate receptors, or reducing the level of $G\alpha_{12/13}$ by MO translation interference resulted in C&E defects. Overexpression of either $G\alpha_{12}$ or $G\alpha_{13}$ CT-peptides caused C&E defects with similar efficiency suggests that signal transduction through both $G\alpha_{12}$ and $G\alpha_{13}$ is essential for these gastrulation movements. However, based on several considerations, we believe that $G\alpha_{12}$ and $G\alpha_{13}$ are functionally redundant in zebrafish gastrulation. First, our MO translation interference experiments showed that gastrulation defects were only observed in embryos injected with the combination of the three MOs to inhibit protein synthesis of $G\alpha_{12}$, $G\alpha_{13}$a, and $G\alpha_{13}$b, but not in embryos injected with the same amount of any single MO. Second, it is well established that $G\alpha_{12}$ and $G\alpha_{13}$ can regulate similar physiological processes via similar signaling pathways (Dhanasekaran and Dermott, 1996; Sah et al., 2000). Indeed, we showed previously that either $G\alpha_{12}$ or $G\alpha_{13}$ CT-peptide could inhibit thrombin receptor-stimulated stress fiber formation in HMEC cells (Gilchrist et al., 2001). Similar results were reported for LPA-mediated stress fiber formation in fibroblasts (Sugimoto et al., 2003). It is possible that $G\alpha_{12}$ and $G\alpha_{13}$ interact with the same receptors in zebrafish gastrulae to regulate C&E. If their binding sites on the receptors are overlapping, it is conceivable that either $G\alpha_{12}$ or $G\alpha_{13}$ CT-peptide is sufficient to block completely signal transduction from both $G\alpha_{12}$ and $G\alpha_{13}$. Finally, the functional redundancy of $G\alpha_{12}$ and $G\alpha_{13}$ in vertebrates is also supported by the findings that compound $G\alpha_{13}$ and $G\alpha_{12}$ mutant mice die earlier (e8.5) than $G\alpha_{13}$ null mice (e9.5), whereas $G\alpha_{12}$ knockout mice are viable (Offermanns, 2001). Together, these findings strongly argue for overlapping functions of $G\alpha_{12}$ and $G\alpha_{13}$ in vertebrates.

In vivo time-lapse analyses revealed that $G\alpha_{12/13}$ signaling is required for several distinct gastrulation cell behaviors, including dorsalward migration and intercalation during C&E movements. However, $G\alpha_{12/13}$ signaling does not appear to act as a general motility factor. Indeed, mesendoderm internalization occurred without any obvious defects in $G\alpha_{12/13}$-depleted gastrulae (unpublished data). Therefore, we conclude that $G\alpha_{12/13}$

signaling affects only a subset of morphogenetic events in zebrafish gastrula. We cannot, however exclude the possibility that there is a residual activity in embryos injected with MOs and or CT-peptides, permitting other morphogenetic processes that require lower levels of $G\alpha_{12/13}$ signaling.

We demonstrated that in $G\alpha_{12/13}$-depleted embryos, mediolateral cell elongation of slowly migrating cells at midgastrulation is impaired, whereas this cell behavior is normal in the *tri* mutant (Jessen et al., 2002). Moreover, our preliminary analyses of lateral mesodermal cells in embryos overexpressing $G\alpha_{13}$ revealed normal cell elongation (unpublished data). This suggests that the role of $G\alpha_{12/13}$ signaling in the regulation of cell elongation is distinct from that of noncanonical Wnt signaling, where either increased or decreased pathway activity impairs elongation of mesodermal cells (Wallingford et al., 2000). Consistent with this hypothesis, our mosaic analyses indicate that mediolateral cell elongation requires only cell-autonomous $G\alpha_{12/13}$ activities, whereas noncanonical Wnt signaling regulates cell elongation both cell-autonomously and nonautonomously (Jessen et al., 2002; Marlow et al., 2002). In addition, ectopic $G\alpha_{12/13}$ activity cannot suppress the $kny^{-/-}$ and $slb^{-/-}$ phenotypes (Fig. 5 and not depicted) and $Fz_{2/7}$ morphant phenotypes (not depicted). Collectively, these results strongly argue that $G\alpha_{12/13}$ do not act as components of a linear noncanonical Wnt signaling pathway to mediate cell polarization. Identification of the ligands and receptors that regulate gastrulation behaviors acting upstream of $G\alpha_{12/13}$ will be our next main focus.

Recent studies indicate that a number of distinct cell behaviors contribute to vertebrate gastrulation (Elul and Keller, 2000; Jessen et al., 2002; Myers et al., 2002b; Montero et al., 2003). How is this diversity of cell behaviors generated? In some gastrula regions, cells are engaged in more than one cell behavior, suggesting that cells are competent to respond to several cues. Our work implicates $G\alpha_{12/13}$ as key mediators of many different gastrulation cell behaviors: slow and fast dorsal convergence in lateral regions and cell intercalation in dorsal regions (Figs. 5 and 7; Jessen et al., 2002; Myers et al., 2002b; Glickman et al., 2003). Given that $G\alpha_{12/13}$ can be activated by a variety of GPCR/ligands, it is tempting to hypothesize that these proteins may underlie interaction with signals in different regions of fish gastrulae to generate the distinct gastrulation cell behaviors. In the lateral region, cells become influenced by a dorsally provided attracting system that initiates convergence movements. Evidence suggests that β-catenin activates the STAT3 pathway in the dorsal gastrula organizer to produce a long range dorsal attractant, which could interact with $G\alpha_{12/13}$ signaling to mediate slow dorsal convergence movements (Yamashita et al., 2002). In the dorsolateral region, $G\alpha_{12/13}$ may also interact with the noncanonical Wnt signaling to generate high mediolateral elongation underlying fast dorsal migration. Finally in the dorsal region, $G\alpha_{12/13}$ and noncanonical Wnt signaling could interact with yet to be identified regulators to mediate intercalation behavior. In conclusion, we establish a central role for $G\alpha_{12}$ and $G\alpha_{13}$ proteins in mediating several distinct cell behaviors that drive vertebrate gastrulation. Identification of extracellular cues that are integrated by $G\alpha_{12/13}$ to mediate individual gastrulation cell behaviors is an important future goal for this research into the molecular mechanisms of morphogenesis.

Materials and methods

Zebrafish maintenance

WT zebrafish of AB*, India, TL and hybrid backgrounds, $slb^{tz216/tz216}$, kny^{m119} (Heisenberg et al., 2000; Topczewska et al., 2001), zebrafish strains were maintained as described previously (Solnica-Krezel et al., 1994). Embryos were obtained from natural mating and staged according to morphology as described previously (Kimmel et al., 1995).

Cloning zebrafish *gna12/13* and generation of $G\alpha_{12/13}$ COOH-terminal peptide constructs

Zebrafish *gna12* and *gna13* cDNAs were cloned by RT-PCR and then subcloned into the pCS_2 expression vector. The conserved glutamine at residue 226 of $G\alpha_{13}$a was changed to leucine to generate a constitutively active form of Gα protein (Katoh et al., 1998) using the QuikChange mutagenesis kit (Stratagene). To generate constructs encoding the last 11 COOH-terminal aa of $G\alpha_S$ (QRMHLRQYELL), $G\alpha_{12}$ (LQENLKDIMLQ), and $G\alpha_{13}$ (LHDNLKQLMLQ), two synthetic short complimentary oligonucleotides encoding the peptide sequences were obtained for each gene. The forward and reverse oligonucleotides were annealed, and subcloned into pCS_2 vector. These constructs were designated as $G\alpha_s$-CT, $G\alpha_{12}$-CT, and $G\alpha_{13}$-CT (one peptide was used to block function of both $G\alpha_{13}$a and $G\alpha_{13}$b because they have identical COOH-terminal sequences). Longer forms of CT peptides encoding the last 50 aa of COOH termini of $G\alpha_{13}$ and $G\alpha_{12}$, which included a HA-tag at the NH_2-terminus, were constructed by PCR. All constructs were verified by DNA sequencing.

Microscopy

Live embryos for still photography were mounted in 1.5–2% methylcellulose at 28°C, whereas embryos processed for whole-mount in situ hybridization were mounted in 75% glycerol/PBT. Embryos were photographed using an Axiophot2 microscope (Carl Zeiss MicroImaging, Inc.) and an Axiocam digital camera (Carl Zeiss MicroImaging, Inc.). For confocal imaging, embryos were mounted in 75% glycerol/PBT, and a laser scanning inverted microscope (model LSM 510; Carl Zeiss MicroImaging, Inc.) with a 40× lens and 2× digital Zoom was used. All images acquired were compiled and edited using Adobe Photoshop and Illustrator software.

In situ hybridization

Sense and antisense RNA probes for *gna12*, *gna13a*, and *gna13b* were synthesized using the NH_2-terminal EST clones as templates. Antisense RNA probes *hgg1*, *dlx3*, *krox20*, *shh*, *deltaC*, *ntl*, *bmp4*, and *chordin* were synthesized as described previously (Jessen et al., 2002). Whole-mount in situ hybridization was performed as described previously (Thisse and Thisse, 1998), except that BM purple (Roche) was used for the chromogenic reaction. Sense probes produced no signal.

Cell culture stress fiber formation assay

HEK cells were transiently transfected with GFP or with G protein constructs as indicated. To block Rok activity, ROCK inhibitor, Y-27623 was added at 10 μM to media after transfection (Uehata et al., 1997). Stress fiber formation assay was performed as described previously (Gilchrist et al., 2001). Anti-$G\alpha_{12}$ or $G\alpha_{13}$ antibodies (1:100) generated against the last 11 AAs of human $G\alpha_{12}$ or $G\alpha_{13}$ (Hallak et al., 1994) were used to identify the G protein–expressing cells. Cells were mounted in Vectashield mounting medium (Vector Laboratories) and confocal images were acquired as described in Microscopy.

Whole-mount immunostaining

Zebrafish embryos were fixed in 4%PFA/PBS/4% sucrose at shield and whole mount immunohistochemistry was performed as described previously (Topczewska et al., 2001). Primary anti-$G\alpha_{12}$ or $G\alpha_{13}$ antibodies and Cy_2-conjugated pAb (1:100) were used. No signal was detected when the primary antibodies were preincubated with the peptides encoding the COOH-terminal 11 residues of the $G\alpha_{12}$ or $G\alpha_{13}$, respectively, or when only the secondary antibody was used. Confocal images were acquired.

RNA and antisense MO injections

Capped sense RNAs encoding the $G\alpha_{13}$, $G\alpha_{12}$, $G\alpha_S$ CT-peptides, mGFP (Wallingford et al., 2000) or a full-length zebrafish $G\alpha_{13}$a and human

$G\alpha_{13}$ were synthesized using mMessage Machine system (Ambion). RNAs were injected into embryos at 1–2 cell stage.

Antisense MOs (Gene-Tools) targeted against the zebrafish *gna12*, *gna13a*, and *gna13b* transcripts were designed according to the manufacturer's suggestions and injected into embryos at 1 cell stage. Two distinct MOs were designed to target either the sequences overlapping the ATG initiation codon (MO1) or the 5′ untranslated sequences (MO2) of *gna13a* transcript. For *gna13b* and *gna12,* one MO against sequence overlapping the translation start site was designed for each transcript.

Time-lapse and cell shape analysis

Nomarski time-lapse images of lateral gastrula mesodermal cells at midgastrulation (80% epiboly) were collected as described previously (Myers et al., 2002a). Dechorionated zebrafish embryos were mounted in 0.8–1% low melting point agarose in 30% Danieau's buffer (100% Danieau's buffer: 58 mM NaCl, 0.7 mM KCl, 0.4 mM $MgSO_4$, 0.6 mM $CaCl_2$, 5 mM Hepes, pH 7.6), to view the lateral mesoderm (90° from the dorsal midline). The microscope room was maintained at 28°C during recordings. Single focal plane time-lapse recordings were collected at 30-s intervals using DIC optics and a 20× objective (0.5 NA Plan Neofluor) on an Axiophot2 microscope (Carl Zeiss MicroImaging, Inc.) and an Axiocam digital camera (Carl Zeiss MicroImaging, Inc.). Images were analyzed using Object-Image software (Norbert Vischer, http://simon.bio.uva.nl/object-image.html). Data was exported to Excel (Microsoft) where cell migration speed, path, direction, turning angle, and LWRs were determined according to Topczewski et al. (2001). The direction of movements of lateral mesodermal cells was determined at 30-s intervals and change in movement direction was calculated. A turn was defined as a change in direction of >60°. We also determined the actual direction of lateral mesendodermal cells at every 60-s interval.

To investigate shape of notochord cells, WT embryos or embryos obtained from *kny*^{m119} heterozygous parents were injected with *mgfp* RNA (Wallingford et al., 2000) alone or with 3MOs, and were then fixed in 4% PFA. Images of notochord were collected on a confocal microscope and LWR of notochord cells and the angle of the long axis relative to a line perpendicular to the embryonic axis as represented by the notochord were analyzed using Object-Image software.

Transplantation experiments

For cell autonomy analyses, cells from embryos injected with dextran-Rhodamine or together with 3MO were transplanted into host embryos injected with *mgfp* RNA and 3MO or *mgfp* RNA alone at 1K-dome stage (*mgfp* RNA was injected to visualize cell shape), as described previously (Jessen et al., 2002). Host embryos were then fixed in 4% PFA at 4s stage and stained with anti-Rhodamine, then LWR and the angle of the long axis of notochord cells relative to a line perpendicular to the embryonic axis were determined.

Statistical analysis

Data are presented as the mean ± 1 SD. Statistical analyses were performed using unpaired *t* tests unequal variance. In all analyses, the asterisk indicates $P < 0.001$.

Accession nos.

GenBank/EMBL/DDBJ accession nos. for the zebrafish *gna12*, *gna13a*, and *gna13b* are AY386359, AY386360, and AY386361, respectively.

Online supplemental material

Fig. S1 shows the sequence alignment of human and zebrafish $G\alpha_{12/13}$. Two synthetic short complementary oligonucleotides encoding the peptide sequences were obtained for *gna12*, *gna13*, and *gnaS*. Online supplemental material is available at http://www.jcb.org/cgi/content/full/jcb.200501104/DC1.

We thank L. Solnica-Krezel and H. Hamm lab members for discussions and J. Jessen, T.P. Wilm, and A. Inbal for critical comments. We acknowledge J. Clanton and A. Bradshaw for excellent fish care. We are grateful to Dr. David Manning (University of Philadelphia) for $G\alpha_{12}$ and $G\alpha_{13}$ antibodies, to C.-P. Heisenberg for *slb* mutant fish, to P. Ingham, M. Ekker, N. Ueno, C. and B. Thisse, M. Halpern, and J. Lewis for probes. Confocal experiments were performed in VUMC Cell Imaging Core facility (supported by National Institutes of Health [NIH] grant 1S10RR015682).

D.S. Sepich is supported by NIH Vascular Biology Training grant (T32HL07751). The work in L. Solnica-Krezel lab is supported by NIH GM55101 grant. H. Hamm lab is supported by NIH grants EY10291 and HL60678.

Submitted: 19 January 2005
Accepted: 26 April 2005

References

Ahumada, A., D.C. Slusarski, X. Liu, R.T. Moon, C.C. Malbon, and H.Y. Wang. 2002. Signaling of rat Frizzled-2 through phosphodiesterase and cyclic GMP. *Science.* 298:2006–2010.

Akhter, S.A., L.M. Luttrell, H.A. Rockman, G. Iaccarino, R.J. Lefkowitz, and W.J. Koch. 1998. Targeting the receptor-$G\alpha_q$ interface to inhibit in vivo pressure overload myocardial hypertrophy. *Science.* 280:574–577.

Arai, K., Y. Maruyama, M. Nishida, S. Tanabe, S. Takagahara, T. Kozasa, Y. Mori, T. Nagao, and H. Kurose. 2003. Differential requirement of $G\alpha_{12}$, $G\alpha_{13}$, $G\alpha_q$, and $G\beta\gamma$ for endothelin-1-induced c-Jun NH2-terminal kinase and extracellular signal-regulated kinase activation. *Mol. Pharmacol.* 63:478–488.

Buhl, A.M., N.L. Johnson, N. Dhanasekaran, and G.L. Johnson. 1995. $G\alpha_{12}$ and $G\alpha_{13}$ stimulate Rho-dependent stress fiber formation and focal adhesion assembly. *J. Biol. Chem.* 270:24631–24634.

Crawford, B.D., C.A. Henry, T.A. Clason, A.L. Becker, and M.B. Hille. 2003. Activity and distribution of paxillin, focal adhesion kinase, and cadherin indicate cooperative roles during zebrafish morphogenesis. *Mol. Biol. Cell.* 14:3065–3081.

Dhanasekaran, N., and J.M. Dermott. 1996. Signaling by the $G\alpha_{12}$ class of G proteins. *Cell. Signal.* 8:235–245.

Elul, T., and R. Keller. 2000. Monopolar protrusive activity: a new morphogenic cell behavior in the neural plate dependent on vertical interactions with the mesoderm in *Xenopus*. *Dev. Biol.* 224:3–19.

Feldman, D.S., A.M. Zamah, K.L. Pierce, W.E. Miller, F. Kelly, A. Rapacciuolo, H.A. Rockman, W.J. Koch, and L.M. Luttrell. 2002. Selective inhibition of heterotrimeric $G\alpha_s$ signaling. Targeting the receptor-G protein interface using a peptide minigene encoding the $G\alpha_s$ carboxyl terminus. *J. Biol. Chem.* 277:28631–28640.

Gilchrist, A., M. Bunemann, A. Li, M.M. Hosey, and H.E. Hamm. 1999. A dominant-negative strategy for studying roles of G proteins in vivo. *J. Biol. Chem.* 274:6610–6616.

Gilchrist, A., J.F. Vanhauwe, A. Li, T.O. Thomas, T. Voyno-Yasenetskaya, and H.E. Hamm. 2001. Gα minigenes expressing C-terminal peptides serve as specific inhibitors of thrombin-mediated endothelial activation. *J. Biol. Chem.* 276:25672–25679.

Glickman, N.S., C.B. Kimmel, M.A. Jones, and R.J. Adams. 2003. Shaping the zebrafish notochord. *Development.* 130:873–887.

Gohla, A., R. Harhammer, and G. Schultz. 1998. The G-protein $G\alpha_{13}$ but not $G\alpha_{12}$ mediates signaling from lysophosphatidic acid receptor via epidermal growth factor receptor to Rho. *J. Biol. Chem.* 273:4653–4659.

Gohla, A., S. Offermanns, T.M. Wilkie, and G. Schultz. 1999. Differential involvement of $G\alpha_{12}$ and $G\alpha_{13}$ in receptor-mediated stress fiber formation. *J. Biol. Chem.* 274:17901–17907.

Habas, R., Y. Kato, and X. He. 2001. Wnt/Frizzled activation of Rho regulates vertebrate gastrulation and requires a novel Formin homology protein Daam1. *Cell.* 107:843–854.

Hallak, H., L. Muszbek, M. Laposata, E. Belmonte, L.F. Brass, and D.R. Manning. 1994. Covalent binding of arachidonate to G protein α subunits of human platelets. *J. Biol. Chem.* 269:4713–4716.

Hamm, H.E. 1998. The many faces of G protein signaling. *J. Biol. Chem.* 273: 669–672.

Hammerschmidt, M., and M.C. Mullins. 2002. Dorsoventral patterning in the zebrafish: Bone morphogenetic proteins and beyond. *In* Pattern Formation in Zebrafish. L. Solnica-Krezel, editor. Springer-Verlag, Berlin Heidelberg. 72–95.

Heisenberg, C.P., M. Tada, G.J. Rauch, L. Saude, M.L. Concha, R. Geisler, D.L. Stemple, J.C. Smith, and S.W. Wilson. 2000. *Silberblick/Wnt11* mediates convergent extension movements during zebrafish gastrulation. *Nature.* 405:76–81.

Jessen, J.R., J. Topczewski, S. Bingham, D.S. Sepich, F. Marlow, A. Chandrasekhar, and L. Solnica-Krezel. 2002. Zebrafish *trilobite* identifies new roles for Strabismus in gastrulation and neuronal movements. *Nat. Cell Biol.* 4:610–615.

Katanaev, V.L., R. Ponzielli, M. Semeriva, and A. Tomlinson. 2005. Trimeric G protein-dependent Frizzled signaling in *Drosophila. Cell.* 120:111–122.

Katoh, H., J. Aoki, Y. Yamaguchi, Y. Kitano, A. Ichikawa, and M. Negishi. 1998. Constitutively active $G\alpha_{12}$, $G\alpha_{13}$ and $G\alpha_q$ induce Rho-dependent neurite retraction through different signaling pathways. *J. Biol. Chem.* 273:28700–28707.

Keller, R. 2002. Shaping the vertebrate body plan by polarized embryonic cell movements. *Science.* 298:1950–1954.

Kimmel, C.B., W.W. Ballard, S.R. Kimmel, B. Ullmann, and T.F. Schilling. 1995. Stages of embryonic development of the zebrafish. *Dev. Dyn.* 203:253–310.

Kinoshita, N., H. Iioka, A. Miyakoshi, and N. Ueno. 2003. PKCδ is essential for Dishevelled function in a noncanonical Wnt pathway that regulates *Xenopus* convergent extension movements. *Genes Dev.* 17:1663–1676.

Kuhl, M., K. Geis, L.C. Sheldahl, T. Pukrop, R.T. Moon, and D. Wedlich. 2001. Antagonistic regulation of convergent extension movements in *Xenopus* by Wnt/β-catenin and Wnt/Ca^{2+} signaling. *Mech. Dev.* 106:61–76.

Lee, Y.N., C.C. Malbon, and H.Y. Wang. 2004. $G\alpha_{13}$ signals via p115RhoGEF cascades regulating JNK1 and primitive endoderm formation. *J. Biol. Chem.* 279:54896–54904.

Liu, T., A.J. DeCostanzo, X. Liu, H. Wang, S. Hallagan, R.T. Moon, and C.C. Malbon. 2001. G protein signaling from activated rat Frizzled-1 to the β-catenin-Lef-Tcf pathway. *Science.* 292:1718–1722.

Liu, X., T. Liu, D.C. Slusarski, J. Yang-Snyder, C.C. Malbon, R.T. Moon, and H. Wang. 1999. Activation of a Frizzled-2/β-adrenergic receptor chimera promotes Wnt signaling and differentiation of mouse F9 teratocarcinoma cells via $G\alpha_{13}$ and $G\alpha_t$. *Proc. Natl. Acad. Sci. USA.* 96:14383–14388.

Malbon, C.C., H. Wang, and R.T. Moon. 2001. Wnt signaling and heterotrimeric G-proteins: strange bedfellows or a classic romance? *Biochem. Biophys. Res. Commun.* 287:589–593.

Marlow, F., J. Topczewski, D. Sepich, and L. Solnica-Krezel. 2002. Zebrafish Rho kinase 2 acts downstream of *Wnt11* to mediate cell polarity and effective convergence and extension movements. *Curr. Biol.* 12:876–884.

Montero, J.A., B. Kilian, J. Chan, P.E. Bayliss, and C.P. Heisenberg. 2003. Phosphoinositide 3-kinase is required for process outgrowth and cell polarization of gastrulating mesendodermal cells. *Curr. Biol.* 13:1279–1289.

Myers, D.C., D.S. Sepich, and L. Solnica-Krezel. 2002a. Bmp activity gradient regulates convergent extension during zebrafish gastrulation. *Dev. Biol.* 243:81–98.

Myers, D.C., D.S. Sepich, and L. Solnica-Krezel. 2002b. Convergence and extension in vertebrate gastrulae: cell movements according to or in search of identity? *Trends Genet.* 18:447–455.

Nasevicius, A., and S.C. Ekker. 2000. Effective targeted gene "knockdown" in zebrafish. *Nat. Genet.* 26:216–220.

Offermanns, S. 2001. In vivo functions of heterotrimeric G-proteins: studies in Gα-deficient mice. *Oncogene.* 20:1635–1642.

Offermanns, S., V. Mancino, J.P. Revel, and M.I. Simon. 1997. Vascular system defects and impaired cell chemokinesis as a result of $G\alpha_{13}$ deficiency. *Science.* 275:533–536.

Parks, S., and E. Wieschaus. 1991. The *Drosophila* gastrulation gene concertina encodes a Gα-like protein. *Cell.* 64:447–458.

Penzo-Mendez, A., M. Umbhauer, A. Djiane, J.C. Boucaut, and J.F. Riou. 2003. Activation of Gβγ signaling downstream of Wnt-11/Xfz7 regulates Cdc42 activity during *Xenopus* gastrulation. *Dev. Biol.* 257:302–314.

Sah, V.P., T.M. Seasholtz, S.A. Sagi, and J.H. Brown. 2000. The role of Rho in G protein-coupled receptor signal transduction. *Annu. Rev. Pharmacol. Toxicol.* 40:459–489.

Sepich, D.S., D.C. Myers, R. Short, J. Topczewski, F. Marlow, and L. Solnica-Krezel. 2000. Role of the zebrafish *trilobite* locus in gastrulation movements of convergence and extension. *Genesis.* 27:159–173.

Sheldahl, L.C., M. Park, C.C. Malbon, and R.T. Moon. 1999. Protein kinase C is differentially stimulated by Wnt and Frizzled homologs in a G-protein-dependent manner. *Curr. Biol.* 9:695–698.

Shih, J., and R. Keller. 1992. Cell motility driving mediolateral intercalation in explants of *Xenopus laevis. Development.* 116:901–914.

Simon, M.I., M.P. Strathmann, and N. Gautam. 1991. Diversity of G proteins in signal transduction. *Science.* 252:802–808.

Solnica-Krezel, L., A.F. Schier, and W. Driever. 1994. Efficient recovery of ENU-induced mutations from the zebrafish germline. *Genetics.* 136: 1401–1420.

Sugimoto, N., N. Takuwa, H. Okamoto, S. Sakurada, and Y. Takuwa. 2003. Inhibitory and stimulatory regulation of Rac and cell motility by the $G\alpha_{12/13}$-Rho and $G\alpha_i$ pathways integrated downstream of a single G protein-coupled sphingosine-1-phosphate receptor isoform. *Mol. Cell. Biol.* 23:1534–1545.

Thisse, C., and B. Thisse. 1998. High resolution whole-mount in situ hybridization. *ZFIN Zebrafish Science Monitor.* 5:8–9.

Topczewska, J.M., J. Topczewski, A. Shostak, T. Kume, L. Solnica-Krezel, and B.L. Hogan. 2001. The winged helix transcription factor Foxc1a is essential for somitogenesis in zebrafish. *Genes Dev.* 15:2483–2493.

Topczewski, J., D.S. Sepich, D.C. Myers, C. Walker, A. Amores, Z. Lele, M. Hammerschmidt, J. Postlethwait, and L. Solnica-Krezel. 2001. The zebrafish glypican *knypek* controls cell polarity during gastrulation movements of convergent extension. *Dev. Cell.* 1:251–264.

Trinkaus, J.P., M. Trinkaus, and R. Fink. 1992. On the convergent cell movements of gastrulation in *Fundulus. J. Exp. Zool.* 261:40–61.

Uehata, M., T. Ishizaki, H. Satoh, T. Ono, T. Kawahara, T. Morishita, H. Tamakawa, K. Yamagami, J. Inui, M. Maekawa, and S. Narumiya. 1997. Calcium sensitization of smooth muscle mediated by a Rho-associated protein kinase in hypertension. *Nature.* 389:990–994.

Ulrich, F., M.L. Concha, P.J. Heid, E. Voss, S. Witzel, H. Roehl, M. Tada, S.W. Wilson, R.J. Adams, D.R. Soll, and C.P. Heisenberg. 2003. *Slb/Wnt11* controls hypoblast cell migration and morphogenesis at the onset of zebrafish gastrulation. *Development.* 130:5375–5384.

Wallingford, J.B., B.A. Rowning, K.M. Vogeli, U. Rothbacher, S.E. Fraser, and R.M. Harland. 2000. Dishevelled controls cell polarity during *Xenopus* gastrulation. *Nature.* 405:81–85.

Wallingford, J.B., S.E. Fraser, and R.M. Harland. 2002. Convergent extension: the molecular control of polarized cell movement during embryonic development. *Dev. Cell.* 2:695–706.

Warga, R.M., and C.B. Kimmel. 1990. Cell movements during epiboly and gastrulation in zebrafish. *Development.* 108:569–580.

Winklbauer, R., A. Medina, R.K. Swain, and H. Steinbeisser. 2001. Frizzled-7 signalling controls tissue separation during *Xenopus* gastrulation. *Nature.* 413:856–860.

Yamashita, S., C. Miyagi, A. Carmany-Rampey, T. Shimizu, R. Fujii, A.F. Schier, and T. Hirano. 2002. Stat3 controls cell movements during zebrafish gastrulation. *Dev. Cell.* 2:363–375.